Simultaneous Observations of Electromagnetic Ion Cyclotron Waves and Longer-Period Ultra Low Frequency Waves by the GOES-16 Magnetometer

T.M. Loto'aniu[1,2], R.J. Redmon[2], M.E. Usanova[3], S. Califf[1,2]

[1]Cooperative Institute for Research in Environmental Sciences, University of Colorado, Boulder, CO, USA.
[2]National Centers for Environmental Information, National Oceanic and Atmospheric Administration, Boulder, CO, USA.
[3]Laboratory for Atmospheric and Space Physics, University of Colorado, Boulder, CO, USA.

Key Points:

- Ion cyclotron wavepacket repetition times associated with variations in solar wind dynamic pressure
- Cross-coupling of ion cyclotron waves and longer-period poloidal ultra low frequency waves during magnetospheric compression
- Longer duration ion cyclotron wave subpackets correlate with longer-period ultra low frequency wave periods

Corresponding author: Paul Loto'aniu, `paul.lotoaniu@noaa.gov`

Abstract

Simultaneous bursts of EMIC and longer-period ULF waves were observed by the GOES-16 magnetometer on the 11 January and the 7 September 2017. No correlation was found between the repeat times of *pearl* EMIC wavepackets and Pc4 ULF wave periods. However, the *pearl* repetition times visually correlated with variations in solar wind dynamic pressure (P_{dyn}). EMIC wavepackets are composed of short duration subpackets and when subpackets last >1/2 the ULF wave period, correlation with the ULF wave cycle was strong, $R^2 = 0.6$. On 11 Jan., observations suggest the Pc5 ULF waves were in-part directly driven by P_{dyn}. The observed Pc4-5 ULF waves were predominately poloidal. Assuming high azimuthal m-numbers, the observations as a whole imply that the simultaneous repeating EMIC and Pc4-5 wave bursts were formed by mode cross-coupling through a common wave generation free energy source of anisotropic ion distributions created by repetitive magnetospheric compressions driven by small P_{dyn} fluctuations.

1 Plain Language Summary

On the 11 January and the 7 September 2017, the magnetometer instrument onboard the GOES-16 spacecraft measured variations in the magnetic field of Earth that are called plasma waves. Two different types of plasma waves were observed simultaneously as repeating wave bursts. In this letter, we study how the waves interacted and the possible ways the two waves may have been created. The results suggest the two wave types can interact under certain circumstances, and that variations in the number of particles coming from the Sun can regulate the reoccurrence of the waves. The results as a whole suggest the energy source needed to generate the two wave types may have been the same, even though the two waves are generated by very different mechanisms. Plasma waves are thought to play a critical role in determining the number of dangerous particles in near-Earth space, and the results of this study indicate that consideration should also be given to how these waves interact with each other in space.

2 Introduction

Ultra low frequency (ULF) waves in the Pc1-5 (2 mHz-5 Hz) range are among the most studied plasma phenomena observed in Earths magnetosphere. The electromagnetic ion cyclotron (EMIC) Pc 1-2 waves ($\sim$ 50 mHz - 5 Hz at GEO orbit) can be categorized into two types: structured and unstructured (Saito, 1969). The structured EMIC waves are frequency band limited, can last from tens of minutes to several hours at mid to high latitudes (Troitskaya, 1961) and are sometimes referred to as *pearl pulsations* as time series magnetograms often show repeating periodic structure that resembles a necklace pearl pattern (Tepley & Landshoff, 1966). Unstructured EMIC waves generally show broadband wave power. EMIC waves are thought to be generated by ion cyclotron instability with the free energy coming from ∼10 of keV anisotropic ion distributions.

Lower frequency Pc4-5 ULF waves ($\sim 2 - 20$ mHz) can be classified in terms of external and internal generation mechanisms (e.g. Baddeley et al., 2002). The external mechanisms such as Kelvin-Helmholtz instability, solar wind buffeting and solar wind pressure variations usually lead to waves with low azimuthal wave numbers, m. High m-number waves are thought to be generated through a wave-particle interaction mechanism such as drift-bounce resonance (Southwood et al., 1969), with the free energy again coming from 10s keV particle distributions.

Previous studies of simultaneous observations of the EMIC waves and lower frequency ULF waves have often concentrated on determining if there is a correlation between EMIC wave *pearl* wavepacket repetition periods or durations and longer-period ULF wave frequencies (e.g. Mursula et al., 1997; Loto'aniu et al., 2009; Usanova et al., 2010; Paulson et al., 2017). These studies have shown mixed results with some suggesting EMIC wave growth rates are modified by the ULF wave cycle varying background magnetic field and/or cold plasma density, while other studies show no correlation. Modeling shows that localized repetitive EMIC wavepackets can be generated through nonlinear means by gyrophase particle bunching due to oppositely propagating EMIC waves (e.g. Omidi et al., 2010). In addition, a similar mechanism may be responsible for EMIC wave modulation of higher frequency, VLF wave growth (Colpitts et al., 2016; Usanova et al., 2018) which provides an interesting avenue for further cross-frequency wave coupling at ion and electron time scales.

In this letter, presented are two plasma wave events observed by the GOES-16 magnetometer where both EMIC and Pc4-5 ULF waves were simultaneously observed. The characteristics of each wave event is described, along with visual similarities and correlations between the two wave modes. Possible generation mechanisms are also discussed. Section 3 very briefly explains the datasets used, Section 4 presents results for the two wave event periods, and Section 5 states conclusions.

3 Instrumentation and Data

This study utilizes 10 samples/s magnetometer (MAG) data from the GOES-16 spacecraft (Loto'aniu et al., 2019). Also used are solar wind data measured by the DSCOVR satellite. The DSCOVR solar wind data is preferred for this study to NASA-OMNI solar wind data because of higher resolution, 3-second sampling compared to NASA-OMNI ∼60-second solar wind particle data. Both the GOES-16 MAG and DSCOVR datasets are available via the NOAA-NCEI data portal [https://www.ngdc.noaa.gov/stp/spaceweather.html]. In order to minimize contamination from higher frequency spacecraft magnetic fields, the GOES-16 MAG instrument includes a 5th-order Butterworth lowpass filter with a 2.5 Hz cutoff, which introduces a frequency dependent phase shift that was removed (See, Loto'aniu et al., 2019, for details on the GOES-16 magnetometer performance). However, the contamination is not significant in the ULF frequency range (Figure 1).

The waves were extracted from the GOES magnetic field data by first converting the data into mean field-aligned (MFA) coordinates. Here, $b_{||}$ is parallel to the local mean magnetic field, defined from a 30-minute running window, b_ϕ azimuthal and positive eastward ($b_{||} \times \hat{r}$, where $\hat{r}$ is the spacecraft location unit vector from Earth), and b_r is radial away from Earth ($b_\phi \times b_{||}$). The ULF waveforms are then extracted by bandpass filtering the data between 3-30 mHz for the 7 Sept. event and 2-10 mHz for the 11 Jan. event, while the EMIC waveforms were extracted by highpass filtering the data with a 0.1 Hz lower cutoff for both events. All the filtering was accomplished using a 5th-order bidirectional Butterworth filter to ensure no phase shift between EMIC and ULF wave cycles were introduced.

The DSCOVR data were ballistically propagated from the satellite location at the 1st Lagrangian point (L1) to the bowshock at Earth. Solar wind conditions during both wave event intervals were mild and therefore ballistic propagation did not introduce significant errors. A known issue on DSCOVR is that density estimates at low values can show significant discrepancies from NASA-OMNI L1 observations. However, this is not a major issue because for this study solar wind dynamic pressure (P_{dyn}) variations are more important than absolute values. P_{dyn} is defined the same as NASA-OMNI as $2 \times 10^{-6} \cdot N \cdot {V_{sw}}^2$ nPa [https://omniweb.gsfc.nasa.gov/ftpbrowser/bow_derivation.html] with N the proton number density in numbers/cm^{-3} and V_{sw} the solar wind speed in km/s.

4 Results

The two wave event periods observed by the GOES-16 magnetometer on 11 January and 7 September 2017 are shown in Figures 1. Starting from the top, panels a and b show the azimuthal magnetic field b_ϕ-component time series for both events filtered to accentuate the Pc1 EMIC waves, panels c and d show corresponding detrended b_ϕ dynamic power spectra up to 1 Hz, panels e and f show the magnetic field radial b_r-component time series for both events filtered to emphasize the Pc4-5 ULF waves, panels g and h show corresponding detrended b_r dynamic power spectra up to 50 mHz, panels i and j display the background magnetic field (b_t) for both events, panels k and l show 30-second time series solar wind dynamic pressure (P_{dyn}) measured by DSCOVR and panels m and n show 3-second resolution dynamic power spectra of P_{dyn}. The lines that streak diagonally across the EMIC wave dynamic power spectra (panels b and c) are due to spacecraft reaction wheel noise. Characteristics of the two wave events are described below.

4.0.1 11 January 2017 Event

On 11 Jan., the GOES-16 magnetometer measured simultaneously occurring Pc1 EMIC waves and lower frequency mainly Pc5 ULF waves between 17-20 UT (∼10.9-13.7 MLT). The Pc5 ULF waves continue beyond 20 UT, while EMIC waves taper away (See, Figures 1a and 1e). EMIC wavepackets are seen in the He+ band (Figure 1c) between ∼0.2-0.4 Hz and Pc5 ULF wave power is concentrated at 2-10 mHz (Figure 1g), centered about 6 mHz. The EMIC wave power was strongest in the transverse direction, with the b_ϕ-component shown. The lower frequency Pc5 ULF waves were predominately poloidal, with the radial b_r-component shown. Coupling to the toroidal shear Alfven mode was observed but is not shown. The event occurred during a period of extended solar wind corotating interaction region (CIR) activity that lasted for many months from 2016 through 2017. During the event, solar wind velocity was low, ∼450 km/s, as was Dst (-20 nT) and Kp (2).

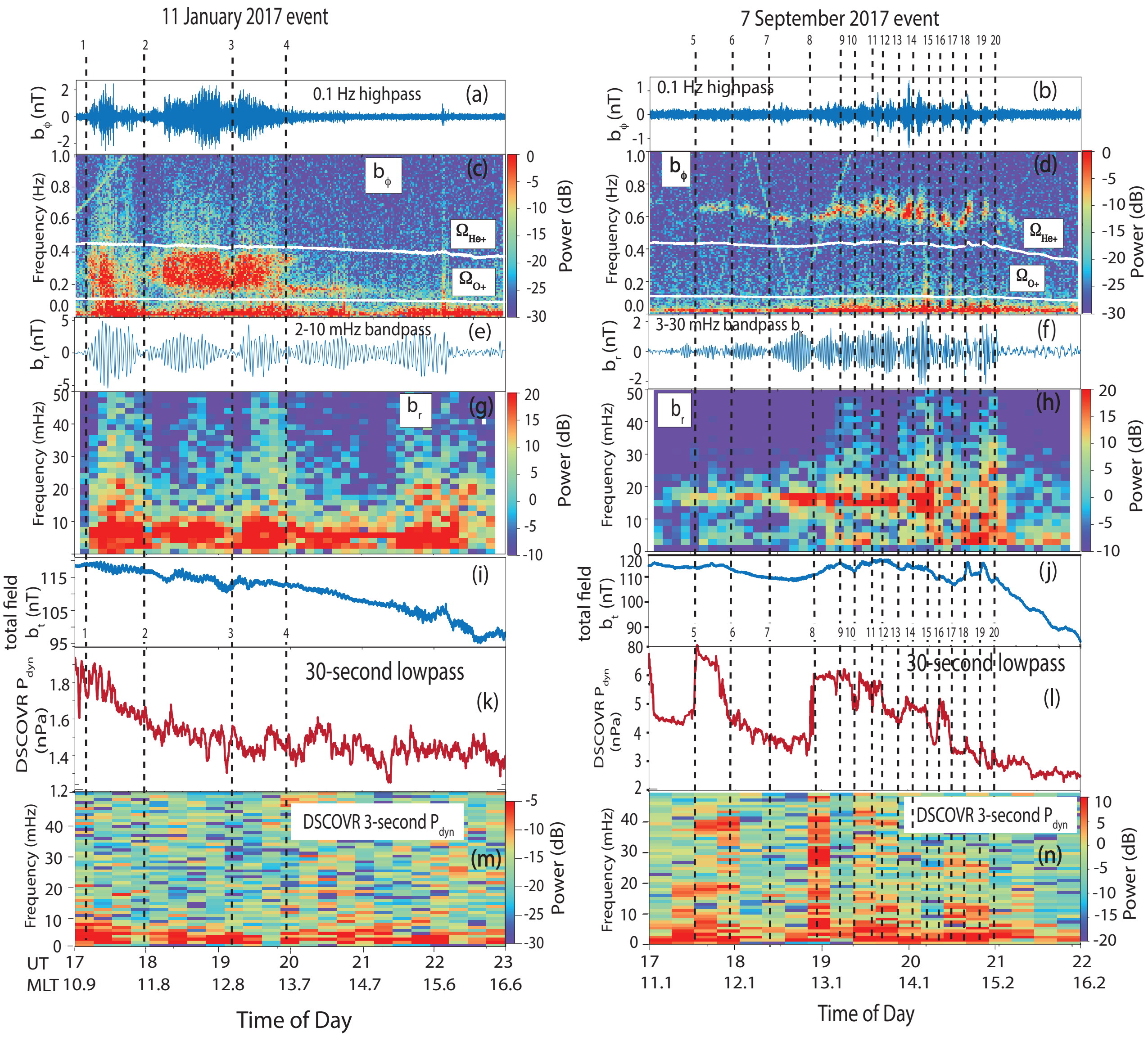

Figure 1. GOES-16 magnetometer and DSCOVR solar wind observations for 11 January and 7 September 2017; $(a-d)$ show the azimuthal magnetic field b_ϕ-component illustrating Pc1 EMIC wave time series and power spectra; $(e-h)$ show the magnetic field radial b_r-component times series and power spectra depicting lower frequency Pc3-5 ULF waves; (i, j) show the total magnetic field (b_t), and $(k-n)$ show 30-second time series and 3-second power spectra solar wind dynamic pressure (P_{dyn}) observed by DSCOVR.

4.0.2 7 September 2017 Event

The second wave event, illustrated on the right-side panels of Figure 1, occurred during the well-studied September 2017 storms (Knipp, 2018). This event was observed between 17-22 UT (11.1-16.2 MLT) on 7 Sept., with observed Pc1 EMIC waves in the H+ band and frequencies between ∼0.5-0.8 Hz (Figure 1d). The EMIC waves showed classic *pearl* wave packet characteristics (e.g. Loto'aniu et al., 2005). The lower frequency ULF waves were predominately observed in the Pc4 range around15-20 mHz (Figure 1h). As with 11 Jan. event, EMIC wave power was predominately transverse (b_ϕ shown) and ULF wave power was predominately poloidal (b_r shown) with coupling to the toroidal shear Alfven mode (not shown). Unlike the 11 Jan. event, EMIC waves in the H+ band on 7 Sept. were observed throughout the period of Pc4 ULF wave observations, and power in the Pc4 range began to dissipate around 20:20 UT.

A coronal mass ejection (CME) arrived at Earth early on 7 Sept. with accompanying enhanced solar wind speed. However, the wave was observed at the tail end of this enhancement where solar wind speed had dropped to ∼500 km/s. The event ended just before the arrival of a second stronger CME. As with the 11 Jan. event., geomagnetic conditions in terms of Dst and Kp were low (not shown) at the time of the event, but they increased dramatically just after the event due to the arrival of the second CME.

4.1 Relating the Plasma Wavepackets to Different Parameters

The vertical dotted lines (numbered $1-20$), in Figure 1, emphasize some interesting features observed in the events. One of these is that bursts of individual Pc4-5 ULF wavepackets tend to be accompanied by bursts of EMIC wavepackets. This is most easily seen when comparing EMIC wave power spectra (Figures 1c and 1d) to corresponding event Pc4-5 ULF wave time series plots (Figures 1e and 1f). For example, for 11 Jan. event, simultaneous bursts in both wave modes can be seen inbetween vertical lines $1-2$, $2-3$ and $3-4$, while for 7 Sept. event this feature is observed between adjacent vertical lines $5-10$. Inbetween vertical lines $10-13$, there are three distinct EMIC wavepacket bursts but the corresponding lower frequency ULF wave time series (Figure 1f) does not show the same amplitude modulation pattern and instead is a continuous ULF wavepacket that lasts until vertical line *13*. Additional simultaneous bursts in both wave modes occur between adjacent vertical lines $13-15$. After this there are still further simultaneous bursts but the frequency of the ULF wave power is more spectrally dispersive (Figure 1h).

Repetitive simultaneous bursts of EMIC and longer period ULF wavepackets, as observed within the vertical dotted lines in Figure 1, suggest a close relationship between the generation and/or modulation of the two wave modes. The equatorial region often provides favorable conditions for EMIC wave generation because of the relatively low ambient background magnetic field that decreases Alfven velocity and proton minimum resonant energy (Criswell, 1969; Gendrin, 1975; Kaye et al., 1979). The GOES-16 satellite orbits near the magnetic equator and likely within the EMIC wave generation region. During 11 Jan. event, there is a ∼4 nT drop in the main field (b_t), as shown in Figure 1i, around the location of vertical lines *2* and *3*, or close to when the second and third major EMIC wavepacket bursts started. However, these background field dips do not last the length of the wavepackets, and for 7 Sept. event there was no obvious correlation between the wavepackets and slow (<< Pc5 ULF wave period) variations in b_t.

The Pc4-5 ULF waves modulate the ambient field, b_t, and previous work has shown a correlation between Pc4-5 wave period and pearl structured EMIC wavepacket duration and/or repetition periods (e.g. Loto'aniu et al., 2009). This idea is based on EMIC wave growth rates increasing during the trough cycle of the lower frequency ULF wave period by lowering the Alfven speed. This mechanism should result in some phase correlation between EMIC wavepacket duration and/or repetition periods and ULF Pc4-5 wave periods.

Inspection by eye of Figure 1 shows no obvious phase correlation between EMIC wavepacket duration/repetition periods and ULF Pc4-5 wave periods, at least not at the resolution shown in the figure. However, each EMIC wavepacket is made up of multiple short duration bursts referred to as subpackets (See, Figure 2c and 2d). Multiple subpackets grouped together create the observed EMIC wavepacket structure seen in Figure 1. Depending on the Fast Fourier Transformation (FFT) length, the subpacket structures may or may not show up in the wave dynamic power spectra. A discussion of the relationship between EMIC wave subpacket durations and ULF wave periods is left to Section 4.2.

Another favorable condition for generation of EMIC waves near local noon is enhanced P_{dyn}. An increase P_{dyn} is thought to support EMIC wave generation by enhancing anisotropic particle distributions due to dayside magnetospheric compression (e.g. Olson & Lee, 1983; Anderson & Hamilton, 1993). Usanova and Mann (2016) observed enhancements in solar wind dynamic pressure and simultaneous compressions in the magnetic field during which GOES also observed bursts of EMIC waves. They found that a ∼4 nPa increase in solar wind dynamic pressure might produce a ∼20% compression resulting in a ∼10% increase in proton temperature anisotropy.

For the 11 Jan. event, Figure 1k shows small variations in P_{dyn} throughout the wave event, while Figure 1m shows that these P_{dyn} variations are in the Pc5-ULF wave band overlapping significant periods when EMIC waves were observed. These P_{dyn} ULF variation amplitudes are very small, for example ∼0.1-0.3 nPa between ∼17-20 UT. However, this maybe enough to trigger EMIC wave growth through ion cyclotron instability because the dayside magnetospheric plasma is often close to marginal stability (Anderson & Hamilton, 1993). These small pressure variations combined with variations in the ambient magnetic field and cold plasma density due to Pc5 waves would result in modulation of EMIC wave growth that was complex, and modeling is required to determine if growth rates could be maintained in such a scenario to produce the EMIC wavepacket structure observed on 11 Jan.

For the 7 Sept. event, variations in P_{dyn} are more easily correlated with EMIC waves, as illustrated by following the vertical lines from Figure 1 panel *d* down to panel *l*. The EMIC waves start when P_{dyn} enhances at line *5*. At line *6*, P_{dyn} relaxes along with EMIC wave power. Immediately after line *6* there is some EMIC wave activity but P_{dyn} momentarily increased by only ∼0.2 nPa. Just after Line *7* new simultaneous Pc4 ULF and EMIC wavepackets start but again there is little P_{dyn} change. At line *8*, P_{dyn} increases significantly along with bursts of EMIC waves. Continuing along in time across the event, EMIC wavepackets tend to start/end whenever P_{dyn} abruptly changes by a few tenths of nPa or more. Interestingly, there are wavepackets generated in the trough of the P_{dyn} amplitude variation such as between lines *12-13* and *15-16*. In these cases, ULF waves may provide additional positive growth through modulation of growth rates. The P_{dyn} variations are small, but nevertheless based on the overall visual correlation between the EMIC wavepacket *pearl* repetitions and P_{dyn} variations for 7 Sept., the authors believe this event is the first observed EMIC wavepacket *pearl* structured event where *pearl* repetitions can be directly associated with variations in solar wind dynamic pressure.

Generation mechanisms for the observed lower frequency Pc4-5 ULF waves can be both external and internal to the magnetosphere. An external mechanism for generation of compressional or poloidal ULF waves is direct driving by solar wind dynamic pressure variations (e.g. Kepko et al., 2002; Kepko & Spence, 2003). As previously mentioned, lower frequency ULF magnetic field wave power for 11 Jan. event was concentrated in the Pc5 ULF band ($<$ 10 mHz), shown in Figure 1g. This was also the frequency band of observed variations in P_{dyn}, as indicated in Figure 1m. The small amplitude pressure variations between 17-20 UT visually show three main bursts that somewhat align with the three Pc5 ULF wavepackets observed in the magnetic field. The Pc5 ULF waves observed by the GOES-16 magnetometer on 11 Jan. could have been directly driven by solar wind dynamic pressure, albeit by small P_{dyn} variations. The frequencies of magnetospheric ULF waves are usually controlled by internal factors, such as magnetic field topology and field line lengths, field line mass loading and other factors (Takahashi, 1998; Yumoto, 1986). Frequencies where peak wave power are observed in the magnetosphere can be different from wave frequencies observed in the solar wind. There is also evidence of wave harmonics in Figure 1g, especially around 17:30 UT and 22 UT, and these could be harmonic signatures due to driving by the fundamental frequencies of the solar wind pressure variations.

Significant P_{dyn} variations in the Pc5 frequency range were also observed during 7 Sept. event, along with harmonics in the Pc3-4 range (See, Figure 1n). At vertical line 5, around the time when Pc4 ULF waves were first observed in the magnetic field data, P_{dyn} wave power was also observed at $\sim$16 mHz. However, throughout the entire wave event, P_{dyn} wave power was not consistently observed at the 15-20 mHz range that magnetic field Pc4 ULF waves were observed. The bulk of the persistent P_{dyn} wave power is at lower Pc5 frequencies. The possibility that the Pc4 ULF waves observed in the magnetic field data may have been driven by harmonics of the Pc5 P_{dyn} variations cannot be ruled out.

Another possible generation mechanism for the lower frequency Pc4-5 ULF waves observed on 11 Jan. and 7 Sept. is the internal mechanism of drift-bounce resonance (Southwood et al., 1969; Chen & Hasegawa, 1988, 1991). Here, usually high azimuthal m-number ULF poloidal waves have periods that resonant with the combined drift-bounce periods of energetic non-Maxwellian ring current particle distributions. The non-Maxwellian distribution can come from pressure gradients and other factors such as substorm particle injections.

Estimations of m-numbers for the observed ULF waves were beyond the scope of this study. However, the observations as a whole suggest cross-coupling of the EMIC and Pc4-5 ULF wave modes, possibly through a mechanism of free energy gain or loss from the same energetic ion distribution. Colpitts et al. (2016) observed cross-coupling between EMIC waves and Whistler waves, but not via the mechanism just mentioned because Whistlers are generated by energetic electrons. Cross-coupling will be further studied in a follow-on paper.

4.2 Relationship Between EMIC Subpacket Duration and Pc4-5 Wave Periods

As previously mentioned, each EMIC wavepacket is actually made up multiple bursts or subpackets. Figure 2 top two panels (a and b) show the two events filtered EMIC and ULF wave time series over the time interval when EMIC wavepackets were most intense, which was from about 17:00-20:00 UT for the 11 Jan. event and 19:20-21:00 UT for the 7 Sept. event. The wave components shown are the radial direction (b_r, orange plots) for ULF waves and azimuthal (b_ϕ, blue plots) for EMIC waves. The 11 Jan. ULF wave amplitudes were larger than those observed on 7 Sept., with amplitude maximum $> \pm 5$ nT versus $\sim \pm 2.5$ nT, respectively, while the EMIC wave amplitudes were comparable.

Figures 2c and 2d show example 10 min intervals of the bandpass magnetic field time series, where subpacket structure in the EMIC waves can be clearly seen in both events. The subpacket structure for the two events shows distinctly different character, as illustrated by zooming in further in Figures 2e and 2f. The 7 Sept. EMIC wave subpackets were observed to gradually change amplitude over many EMIC wave cycles, while 11 Jan. EMIC subpacket amplitudes can change abruptly even doubling in amplitude over just one wave cycle. The duration of 11 Jan. EMIC wave subpackets at enhanced amplitudes are random but when a spike in amplitude reaches ≥ 1.5 nT they tend to drop back down again to below 1.5 nT just as quickly. Outside these enhanced time periods low level EMIC amplitudes of a few tenths of nT can last for many minutes. Hence, the reason why the EMIC wave power in Figure 1c for 11 Jan. event shows long duration EMIC wave bursts. The 7 Sept. EMIC wave subpackets tend to either merge into an-

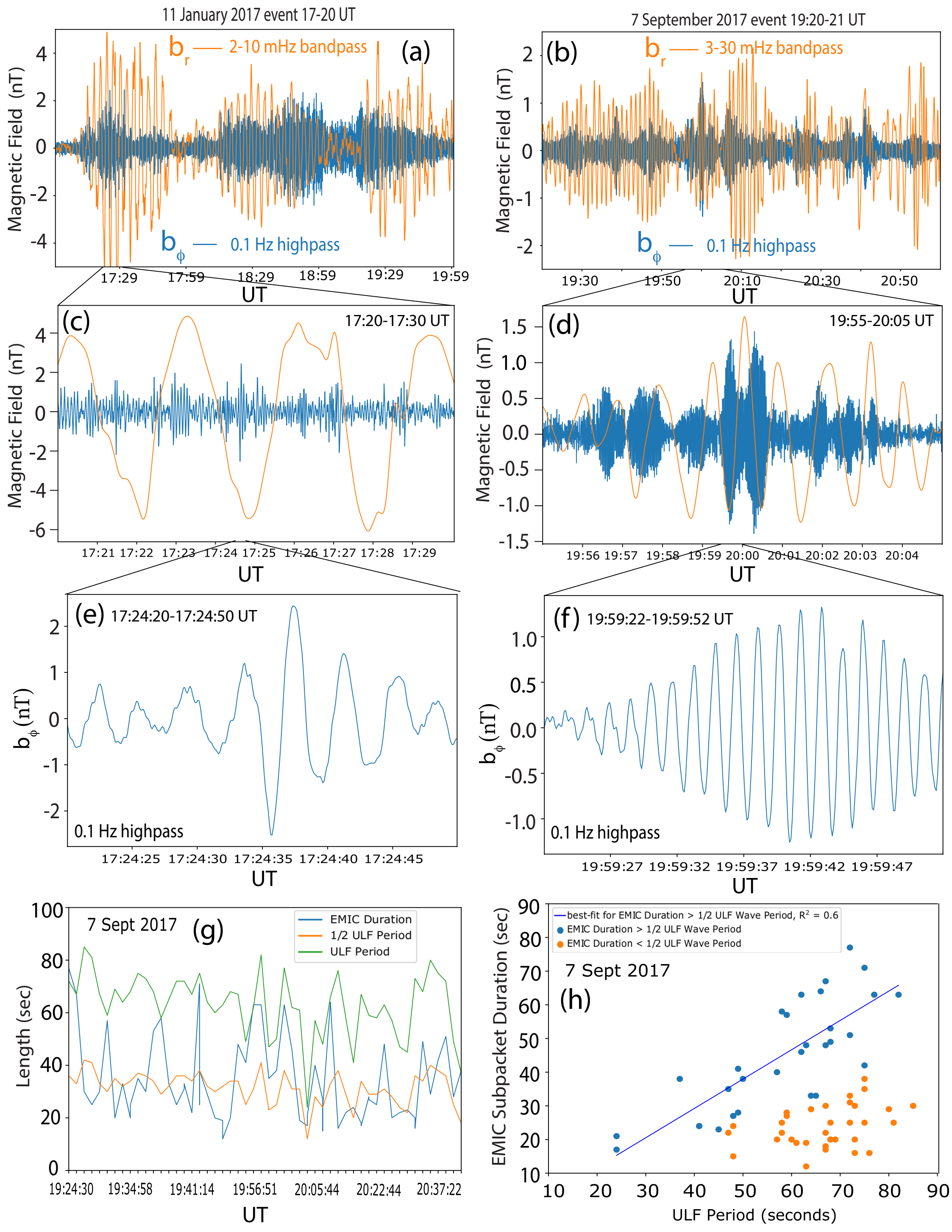

Figure 2. GOES-16 magnetometer (a)-(b) time series for both events showing ULF (orange) and EMIC (blue) waves, (c)-(d) zoomed in to about 10 minutes of times series for both events to show subpacket structure, (e)-(f) further zooming into time series shows difference in how amplitude can change, (g) 7 September event plot of EMIC wave packet duration, ULF wave period and 1/2 ULF wave period and (h) scatter plot of EMIC wave duration vs. ULF wave period split into blue dots for duration greater than 1/2 ULF wave period and orange dots for those less than 1/2 ULF wave period.

other new growing subpacket as observed around 20 UT in Figure 2d, or they have a start/finish amplitude that is close to zero nT as illustrated at the beginning of Figure 2f.

Sudden changes in EMIC wave amplitude like those observed on 11 Jan. usually indicates nonlinear wave growth. Omidi et al. (2010) simulated *pearl* EMIC wavepackets through nonlinear wave evolution attributed to gyrophase cold particle bunching caused by oppositely propagating EMIC waves interacting. The modeled transverse EMIC wavepacket durations were <30 seconds, which are more comparable to the subpacket durations illustrated in Figure 2c and 2d rather than long duration wavepackets shown in Figure 1 that last minutes. The simulated packets also exhibited gradual amplitude changes more in line with 7 Sept. event as opposed to 11 Jan. event subpackets, where no consistency in subpacket repetition structure was observed.

The EMIC subpacket durations were correlated to simultaneous ULF wave periods. However, due to the lack of consistent repetitive structure of the EMIC wave subpackets observed on 11 Jan., subpacket duration times were difficult to objectively determine for that event. Hence, only 7 Sept. event was used to correlate the ULF wave period to EMIC wave subpacket durations.

The 7 Sept. event EMIC subpacket durations and simultaneously observed ULF wave periods are indicated in Figure 2g over the time period shown in Figure 2b. The orange line indicates 1/2 the observed ULF wave period. Subpackets below 10 second duration were not considered in order to place a limit on the number of EMIC wave cycles required to be considered a subpacket. Results in Figure 2g show that on 7 Sept., EMIC subpacket durations tended to either be close to the corresponding simultaneously observed ULF wave cycle period or they tended to last shorter than 1/2 that ULF wave cycle period.

Figure 2h shows a scatter plot of 7 Sept. event EMIC subpacket durations plotted against ULF wave cycle periods. The orange dots indicate subpacket durations lasting below 1/2 the period of simultaneously observed ULF waves, while the blue dots represent EMIC wave subpacket durations lasting $\geq$1/2 the period of the ULF waves. The blue straight line is the line-of-best fit for the blue dots. Considering all subpacket durations, there is no correlation with ULF wave periods except that the longer period Pc4 ULF waves seem to set a limit on the duration of the EMIC subpacket. If you consider only the EMIC subpackets lasting ≥1/2 the ULF wave periods, then the subpacket durations and ULF wave periods show strong correlation, with $R^2 = 0.6$.

Over the entire simulation period studied by Omidi et al. (2010), they found that EMIC wave amplitudes decreased by about 50% after about 1000 proton gyroperiods and remained nearly constant thereafter for hours. Using the proton cyclotron frequency during 7 Sept. event, 1000 gyroperiods corresponds to ∼9.5 min, which is within the individual EMIC wavepacket duration times of 8-12 minutes shown in Figure 1d between about 19:20-21 UT. However, for the 7 Sept. event the wave amplitudes inbetween EMIC wavepackets usually drop close to zero nT. The possible modulation of anisotropic conditions through changing P_{dyn} (as seen in Figure 1l) combined with modulation of Alfven speed and cold plasma density from simultaneously observed lower frequency ULF waves were not considered in the Omidi et al. (2010) study. Future simulations of EMIC waves should take into account the effects of small pressure variations on anisotropic energetic particle distributions along with modulation by ULF waves of the Alfven speed and cold plasma density that may modify the phase bunching conditions and therefore modify the subpacket characteristics.

5 Conclusions

The simultaneity of repeated wave bursts in the Pc1 EMIC and Pc4-5 ULF modes around local noon presents the intriguing possibility of wave mode cross-coupling through having a common free energy source of tens of keV ions. EMIC waves can be generated near local noon through ion cyclotron instability as a result of anisotropic particle distributions due to magnetospheric compression. The observe P_{dyn} variations are small (a few tenths of nPa in most cases), but this was perhaps enough to trigger EMIC wave generation because the dayside magnetospheric plasma is often close to marginal stability (Anderson & Hamilton, 1993; Gary et al., 1993). Small P_{dyn} variations in the Pc4-5 ULF range or sub-harmonics thereof provide seed background noise, while ion drift-bounce resonant instability (Southwood et al., 1969; Chen & Hasegawa, 1988, 1991) might deliver the mechanism for these small variations to grow into poloidal Pc4-5 ULF waves. This latter mechanism usually requires high azimuthal wave m-numbers, which were not estimated for the events. In addition, no energetic particle data was presented. Both particle observations and m-number estimates will be analyzed in a follow-on study.

As far as the authors are aware, results from 7 Sept. where small variations in P_{dyn} visually correlate with the repetition periods of *pearl* structured EMIC wavepacket bursts (See, Figure 1d and 1l), is the first published example of such an event. When EMIC subpacket durations last ≥1/2 the period of simultaneously occurring ULF waves, the subpacket durations correlate with ULF wave periods. One take away from 7 Sept. results is that when modeling *pearl* EMIC waves multiple scale sizes should be considered. There are wavepackets that can last minutes and these wavepackets are made up of subpackets with durations of ∼10s of seconds. These two EMIC wave characteristics are possibly produced by different mechanisms and both need to be explained. For the 11 Jan. EMIC waves, there is no explanation for why the subpackets are more unstructured or what causes the observed sudden changes in subpacket amplitudes over just one or two wave cycles.

At time of writeup, two of the four GOES-R series spacecraft (GOES-16 and GOES-17) had been launched. The magnetometers on GOES-R allow higher frequency, up to 2.5 Hz bandwidth, observations compared to previous GOES satellite series magnetometers that were limited to 0.5 Hz bandwidth. This broader range allows for observing the majority of ULF waves up to the proton cyclotron frequency at geostationary orbit, and with the GOES-R series scheduled to be operational until 2036 the GOES-R magnetometer data should be an important new dataset for plasma wave studies in the magnetosphere.

6 Acknowledgements

We wish to acknowledge and thank the members of the University of Colorado CIRES GOES-R space weather group for their support to the CU-CIRES NCEI MAG group. This work was supported through funding from NOAA-NCEI as part of the GOES-R program calibration working group. Both the GOES-16 MAG and DSCOVR datasets are available via the NOAA-NCEI data portal https://www.ngdc.noaa.gov/stp/spaceweather.html.

References

Anderson, B. J., & Hamilton, D. C. (1993). Electromagnetic ion cyclotron waves stimulated by modest magnetospheric compressions. *Journal of Geophysical Research: Space Physics*, *98*(A7), 11369-11382. Retrieved from https://agupubs.onlinelibrary.wiley.com/doi/abs/10.1029/93JA00605 doi: 10.1029/93JA00605

Baddeley, L. J., Yeoman, T. K., Wright, D. M., Davies, J. A., Trattner, K. J., & Roeder, J. L. (2002). Morning sector drift-bounce resonance driven ulf waves observed in artificially-induced hf radar backscatter. *Annales Geophysicae*, *20*(9), 1487–1498. Retrieved from https://www.ann-geophys.net/20/1487/2002/ doi: 10.5194/angeo-20-1487-2002

Chen, L., & Hasegawa, A. (1988). On magnetospheric hydromagnetic waves excited by energetic ring-current particles. *Journal of Geophysical Research: Space Physics*, *93*(A8), 8763-8767. Retrieved from https://agupubs.onlinelibrary.wiley.com/doi/abs/10.1029/JA093iA08p08763 doi: 10.1029/JA093iA08p08763

Chen, L., & Hasegawa, A. (1991). Kinetic theory of geomagnetic pulsations: 1. internal excitations by energetic particles. *Journal of Geophysical Research: Space Physics*, *96*(A2), 1503-1512. Retrieved from https://agupubs.onlinelibrary.wiley.com/doi/abs/10.1029/90JA02346 doi: 10.1029/90JA02346

Colpitts, C. A., Cattell, C. A., Engebretson, M., Broughton, M., Tian, S., Wygant, J., ... Thaller, S. (2016). Van allen probes observations of cross-scale coupling between electromagnetic ion cyclotron waves and higher-frequency wave modes. *Geophysical Research Letters*, *43*(22), 11,510-11,518. Retrieved from https://agupubs.onlinelibrary.wiley.com/doi/abs/10.1002/2016GL071566 doi: 10.1002/2016GL071566

Criswell, D. R. (1969). Pc1 micropulsations activity and magnetospheric application of 0.2 and 5.0 hz hydomagnetic waves. *J. Geophys. Res.*, *74*, 205.

Gary, S. P., Fuselier, S. A., & Anderson, B. J. (1993). Ion anisotropy instabilities in the magnetosheath. *Journal of Geophysical Research: Space Physics*, *98*(A2), 1481-1488. Retrieved from https://agupubs.onlinelibrary.wiley.com/doi/abs/10.1029/92JA01844 doi: 10.1029/92JA01844

Gendrin, R. (1975). Is the plasmapause a preferential region for proton precipitation? *Annals of Geophys.*, *31*, 127.

Kaye, S. M., Kivelson, M. G., & Southwood, D. (1979). Evolution of ion cyclotron instability in the plasma convection systems of the magnetosphere. *J. Geophys. Res.*, *84*, 6397.

Kepko, L., & Spence, H. E. (2003). Observations of discrete, global magnetospheric oscillations directly driven by solar wind density variations. *Journal of Geophysical Research: Space Physics*, *108*(A6). Retrieved from https://agupubs.onlinelibrary.wiley.com/doi/abs/10.1029/2002JA009676 doi: 10.1029/2002JA009676

Kepko, L., Spence, H. E., & Singer, H. J. (2002). Ulf waves in the solar wind as direct drivers of magnetospheric pulsations. *Geophysical Research Letters*, *29*(8), 39-1-39-4. Retrieved from https://agupubs.onlinelibrary.wiley.com/doi/abs/10.1029/2001GL014405 doi: 10.1029/2001GL014405

Knipp, D. (Ed.). (2018). *Space weather events of 4-10 september 2017* (Vol. 17). Space Weather Journal. Retrieved from https://agupubs.onlinelibrary.wiley.com/doi/toc/10.1002/(ISSN)1542-7390.SW-SEPT2017

Loto'aniu, T. M., Fraser, B. J., & Waters, C. L. (2005). Propagation of electromagnetic ion cyclotron wave energy in the magnetosphere. *Journal of Geophysical Research: Space Physics*, *110*(A7), n/a–n/a. Retrieved from http://dx.doi.org/10.1029/2004JA010816 (A07214) doi: 10.1029/2004JA010816

Loto'aniu, T. M., Fraser, B. J., & Waters, C. L. (2009). The modulation of electromagnetic ion cyclotron waves by pc 5 ulf waves. *Annales Geophysicae*, *27*(1), 121–130. Retrieved from https://www.ann-geophys.net/27/121/2009/ doi: 10.5194/angeo-27-121-2009

Loto'aniu, T. M., Redmon, R. J., Califf, S., Singer, H. J., Rowland, W., Macintyre, S., … Todirita, M. (2019). The goes-16 spacecraft science magnetometer. *Space Science Reviews*, *215*(4), 32. Retrieved from https://doi.org/10.1007/s11214-019-0600-3 doi: 10.1007/s11214-019-0600-3

Mursula, K., Rasinkangas, R., Bosinger, T., Erlandson, R. E., & Lindqvist, P. A. (1997). Nonbouncing pc 1 wave bursts. *J. Geophys. Res.*, *102*, 17611–17624.

Olson, J., & Lee, C. (1983). Pc1 wave generation by sudden impulses. *Planetary Space Sci.*, *31*, 295.

Omidi, N., Thorne, R. M., & Bortnik, J. (2010). Nonlinear evolution of emic waves in a uniform magnetic field: 1. hybrid simulations. *Journal of Geophysical Research: Space Physics*, *115*(A12). Retrieved from https://agupubs.onlinelibrary.wiley.com/doi/abs/10.1029/2010JA015607 doi: 10.1029/2010JA015607

Paulson, K. W., Smith, C. W., Lessard, M. R., Torbert, R. B., Kletzing, C. A., & Wygant, J. R. (2017, jan). In situ statistical observations of pc1 pearl pulsations and unstructured emic waves by the van allen probes. *Journal of Geophysical Research: Space Physics*, *122*(1), 105–119. Retrieved from http://doi.wiley.com/10.1002/2016JA023160 doi: 10.1002/2016JA023160

Saito, T. (1969). Geomagnetic pulsations. *Space Science Rev.*, *13*, 319.

Southwood, D., Dungey, J., & Etherington, R. (1969). Bounce resonant interaction between pulsations and trapped particles. *Planetary and Space Science*, *17*(3), 349 - 361. Retrieved from http://www.sciencedirect.com/science/article/pii/0032063369900683 doi: https://doi.org/10.1016/0032-0633(69)90068-3

Takahashi, K. (1998). Ulf waves: 1997 iaga division 3 reporter review. *Annales Geophysicae*, *16*(7), 787–803. Retrieved from https://www.ann-geophys.net/16/787/1998/ doi: 10.1007/s00585-998-0787-1

Tepley, L., & Landshoff, R. (1966). Waveguide theory for ionospheric propagation of hydromagnetic emissions. *J. Geophys. Res.*, *71*, 1499.

Troitskaya, V. (1961). Pulsations of the earth's electromagnetic field with periods of 1 to 15 s and their connection with phenomena in the high atmosphere. *J. Geophys. Res.*, *66*, 5.

Usanova, M. E., Ahmadi, N., Malaspina, D. M., Ergun, R. E., Trattner, K. J., Reece, Q., … Burch, J. L. (2018). Mms observations of harmonic electromagnetic ion cyclotron waves. *Geophysical Research Letters*, *45*(17), 8764-8772. Retrieved from https://agupubs.onlinelibrary.wiley.com/doi/abs/10.1029/2018GL079006 doi: 10.1029/2018GL079006

Usanova, M. E., & Mann, I. R. (2016, 11). Understanding the role of emic waves in radiation belt and ring current dynamics: Recent advances: A complex interplay. In (p. 244-276). Oxford Scholarship Online. doi: 10.1093/acprof:oso/9780198705246.003.0011

Usanova, M. E., Mann, I. R., Kale, Z. C., Rae, I. J., Sydora, R. D., Sandanger, M., … Vallières, X. (2010). Conjugate ground and multisatellite observations of compression-related emic pc1 waves and associated proton precipitation. *Journal of Geophysical Research: Space Physics*, *115*(A7). Retrieved from https://agupubs.onlinelibrary.wiley.com/doi/abs/10.1029/

2009JA014935 doi: 10.1029/2009JA014935

Yumoto, K. (1986, December). Generation and propagation mechanisms of low-latitude magnetic pulsations - A review. *Journal of Geophysics Zeitschrift Geophysik*, *60*, 79-105.